DUST–GAS INTERRELATIONS IN COMETS: OBSERVATIONS AND THEORY

MICHAEL R. COMBI*, KONSTANTIN KABIN, DARREN L. DeZEEUW and TAMAS I. GOMBOSI

*Space Physics Research Laboratory, Department of Atmospheric Oceanic and Space Sciences, 1417 A Space Research Building, The University of Michigan, Ann Arbor, MI 48109-2143, USA (*E-mail: mcombi@umich.edu)*

KENNETH G. POWELL

W. M. Keck Foundation CFD Laboratory, Department of Aerospace Engineering, The University of Michigan, Ann Arbor, MI 48109, USA

(Received 23 February 1998; Accepted 6 August 1998)

Abstract. The development of the expanding atmosphere from the evaporating cometary nucleus has traditionally focused on observing and modeling the separate development of two distinct components, gas and dust, which are coupled dynamically with one another at distances out to a few tens of cometary radii. In the last decade or so, however, direct evidence from observations and suggestions from theory suggest that the dusty-gas coma is a tightly coupled system where material is transferred between the solid and gaseous phase as an important integral part of the basic development of the coma.

Comet Hale–Bopp (C/1995 O1) was discovered far from the sun and is the largest and most productive comet, in the sense of release of gas and dust in modern times. This has permitted observations to be made over an unprecedented range of heliocentric distance. This paper presents a review of a range of important issues regarding interrelations between dust and gas in comets, a description of the gas and dust environment for Hale–Bopp, and a summary of the preliminary results from Hale–Bopp which are relevant to these issues. Particular topics include dusty-gas models, dust fading and fragmentation, the role of dust and gas jets, the day/night distribution of gas and dust, and extended sources of gas.

Keywords: Comets, Hale–Bopp, dynamics, photochemistry

1. Introduction

Historically, the term comet has been given to the expanding atmosphere of neutral and ionized gas and dust surrounding a small icy parent body (the nucleus) which is in an eccentric orbit around the sun and which shows a head (or coma) and one or more tails. It is understood that evaporation of volatile ices from the comet's nucleus, the release of particulate material (dust), and the subsequent interaction between dust and gas in its immediate vicinity (within a few nucleus radii) are responsible for the observed phenomena. For comet P/Halley we do have spacecraft images of the dust distribution in this region. In general, however, the

Earth, Moon and Planets **79:** 275–306, 1997.

innermost coma serves as an unresolved black box source for the gas and dust observed remotely outside this region. The detailed connection between the icy parent body and the black-box source of gas and dust remains clouded. There is still an incomplete picture regarding the overall nature of the conditions and processes occurring in the innermost coma. As will be discussed in detail below, recent evidence has blurred the traditional separation between the dust and gas components of the coma, indicating that not only are they dynamically coupled to one another but possibly together form a tightly coupled system. There is strong observational evidence for the production of extended non-nuclear sources of gas species which might come from dust or icy grains, and there are theoretical suggestions of recondensation of gases back into icy grains.

Comet Hale–Bopp (C/1995 O1) was discovered far from the sun and is the largest and most productive comet, in the sense of release of gas and dust, in modern times. This, combined with continued advances in ground-based and near-Earth-based instrumentation, has permitted an unprecedented range and quality of remote observations of gas and dust to be obtained. Because the geocentric distance for Hale–Bopp was never very small, this inner region is typically unresolved, and therefore continued progress in our understanding of the important innermost coma requires a combination of observational evidence of gas and dust exiting this region and theoretical modeling which accounts for the basic physics and chemistry. Observations of comet Hale–Bopp which provide new insight into the interrelations between gas and dust in the coma are summarized. Theoretical modeling developments in the study of dusty-gas dynamics are also discussed. Particular topics include dusty-gas models, dust fading and fragmentation, the role of dust and gas jets, the day/night distribution of gas and dust, and extended sources of gas.

2. The Gas–Dust Environment of Comet Hale–Bopp

Most coma modeling has been performed either for rather faint, to moderate, to so-called bright (P/Halley) comets. The very large production rate of Hale–Bopp introduces some interesting physical effects which are usually not very important in other comets and are often totally ignored in the interpretation of data. The first obvious difference is the large collisional coma. A typical definition for the collisional zone of a spherical coma is that distance where the local collisional mean free path is equal to the distance from the center of the nucleus. For example Whipple and Huebner (1976) give

$$R_{\rm coll} = \frac{Q_{\rm gas}\sigma}{4\pi v}.$$

For the conditions of a Halley-class comet at 1 AU, a total gas production rate, $Q_{\rm gas} = 7 \times 10^{29}$ s^{-1}, a nominal collision cross section of $\sigma = 3 \times 10^{-15}$ cm^2, and an outflow velocity of about 0.9 km s^{-1}, the collision zone radius is about

1.9×10^4 km. For comet Hale–Bopp near perihelion the total gas production rate is close to 10^{31} s^{-1}. All else being equal, this would yield a collision sphere of about 2.7×10^5 km. The primary heating agent of the neutral coma is the collisional thermalization of the energy imparted to hot H atoms produced in the main branch of water photodissociation. In a Halley-class comet, because of the 20-to-1 mass ratio between H atoms and the average heavy molecule, the H atoms actually begin to decouple collisionally at ∼10% of the typical collision zone radius, producing a moderating effect on photochemical heating which is dependent on the magnitude of the gas production rate. This was first treated in the context of hydrodynamic models using heuristic approximations (Ip, 1983; Kitamura, 1986), escape probabilities (Huebner and Keady, 1983), and multifluids for pre-thermal and thermalized H (Marconi and Mendis, 1984). Later iterative Monte Car1o-type kinetic models for H atoms were developed to explicitly calculate the collisional efficiency (Combi, 1987; Bockelée-Morvan and Crovisier, 1987; Combi and Smyth, 1988; Ip, 1989). The combination of the variations of photochemical heating rate and the overall gas production rate with heliocentric distance is responsible for the variation of the terminal outflow speed of molecules and radicals in the outer coma. The large collision sphere implies that comet Hale–Bopp should have had a much larger region of photochemical heating resulting in higher gas kinetic temperatures and larger outflow speeds. A second related effect of the large gas densities is that infrared radiative cooling is effectively shut-off for the entire collisional coma (Bockelée-Morvan and Crovisier, 1987), thereby further enhancing the effect of the photochemical heating on the coma temperature and outflow speed.

The last important effect of the large coma densities on the expected behavior of the coma is the non-negligible opacity of ionizing and dissociating solar ultraviolet radiation into the inner coma. Marconi and Mendis (1984) had calculated a 1D multifluid spherical coma model for comet Halley conditions, with a self-consistent calculation of the effect of UV opacity in three UV wavelength bands which are primarily responsible for the main photodecay branches of water:

1. $\lambda < 1860$ Å: H + OH,
2. $\lambda < 1450$ Å: H_2 + $O(^1D)$,
3. $\lambda < 984$ Å: ionization (mostly H_2O^+).

The half-power points of their radial profiles of UV attenuation serves a good indicator of the typical distance for shielding the inner coma from incoming UV solar radiation in each wavelength band. If their results are scaled from the production rate in Halley to that of Hale–Bopp at 1 AU, shielding distances of 600, 1100, and 3300 km in each of the three wavelength bands, respectively, are found. This means that in the case of a spherical coma for comet Hale–Bopp ionization will be effectively shut off within ∼3300 km of the nucleus (and in a cylindrical shadow extending to ∼60 000 km antisunward given the size of the Sun's disk). Photodissociations will similarly be shut-off within about 800 km of the nucleus, and the ratios between the various branches will be modified within distances of ∼1000 km. For a non-spherical coma, for instance where the gas production is

skewed primarily sunward and in narrow jets, local effects could be even stronger because of the higher concentrations of gas density. The increased opacity could have consequences on extracting parent production rates or interpreting spatial profiles obtained from very high spatial resolution observations of daughter radicals near the nucleus.

Using a 1D-spherical hybrid kinetic/dusty-gas-hydrodynamic calculation with a fairly simple composition, the gas velocity and temperature have been calculated for a range of heliocentric distances for conditions appropriate for comet Hale–Bopp. This formulation accounts for a water-driven photochemistry, which should be dominant even for fairly large heliocentric distances. The kinetic portion of the calculation is a Monte Carlo model that explicitly accounts for the collisional efficiency of hot H atoms from the main water dissociation, and is solved iteratively with the 1D-spherical steady-state equations for mass, momentum, and energy assuming an ideal gas. The detailed parameters (lifetimes, branching ratios, collision cross sections) have been discussed at length already (Combi and Smyth, 1988; Combi, 1989; Combi and Feldman, 1993). For these models a nucleus radius of 25 km is adopted and the gas coma is assumed to be composed of 80% H_2O, 16.5% CO, and 3.5% CO_2. The CO and CO_2 are included mainly to raise the mean molecular mass to the correct level (about 20 amu). All of the dust is assumed to have a mean size of 0.65 μm. Past calculations for P/Halley (Combi, 1989) produced reasonable results for both the velocity of the gas and the dust particles using only a single dust size of 0.65 μm and a density of 1 g cm^{-3} which gave equivalent results to using an entire more realistic distribution of dust sizes and size dependent particle bulk density (Gombosi et al., 1986). For the calculations presented here a dust-to-gas ratio of 5 times that of Halley was adopted, as is indicated in photometric measurements of $Af\rho$ by Schleicher et al. (1997). As will be discussed below, $Af\rho$ is only a good indicator of the abundance of visible wavelength (half-micron) sized particles, and is only related to the real dust-to-gas ratio given some particle size and terminal velocity distributions. The calculation accounts for the UV optical depth of the water photodissociation rate which is effectively shut off in the inner coma for distances ranging from 800 km at 1 AU to only 35 km at 3 AU. Table I gives the assumed parameters used for the particular calculations.

Figure 1 shows the variation of the gas radial outflow velocity and the gas kinetic temperature as a function of distance from the center of the nucleus for the model calculations. The temperature shows the typical drop to very low values at a few hundred km caused by the dominance of the pressure-driven expansion. The precise form of the drop is a balance between the expansion-cooling and dust–gas heating in the inner coma and photochemical heating in the outer coma. Because of the large production rate, rather larger outflow speeds for parent molecules are expected to be found for Hale–Bopp than for Halley at comparable heliocentric distances. These are produced by increased photochemical heating efficiency resulting

TABLE I
Hybrid kinetic dusty gas hydrodynamic model

r (AU)	$Q(H_2O)$ (10^{28} s^{-1})
3	40
2.5	70
2	140
1.5	200
1	800

from the more complete thermalization of hot H atoms, as well as by increased gas heating by the dust in the inner coma caused by the large dust-to-gas ratio.

These model results compare favorably to early observations from which outflow velocity and temperature of the coma have been determined. Biver et al. (1997a,b) derived mean coma outflow speeds and rotational temperatures from their mm and sub-mm observations of CO and CH_3OH at IRAM and JCMT corresponding to beam aperture full-width-half-maxima (FWHM) in the range of 10 to 26 arcsec. At least in the inner coma, which is primarily sampled by these measurements, the large collision rates discussed above, should maintain a reasonable equilibrium between the gas kinetic and rotational temperatures. We have integrated the mean radial outflow velocity and mean gas kinetic temperature from the results obtained from the 1-D model over a Gaussian beam of 14 arcsec (the intermediate size for the observations) at the appropriate pre- and post-perihelion geocentric distances and fitted them to power-law variations with heliocentric distance for comparison with the results of Biver et al. They found pre- and post-perihelion velocities in km s^{-1} of $1.18r^{-0.44}$ and $1.07r^{-0.37}$, and rotational temperatures of $116r^{-1.24}$ and $93r^{-0.83}$ in Kelvin. Here, r is the heliocentric distance in AU. For the corresponding model values we find pre- and post- perihelion velocities of $1.01r^{-0.32}$ and $1.02r^{-0.34}$ and temperatures of $114r^{-1.6}$ and $117r^{-1.6}$. The small differences between pre- and post-perihelion results from the model are due to the differences in geocentric distance for corresponding observations before and after perihelion. The agreement between model and observations for the mean outflow speed is quite good. Perhaps this should not be too surprising because the same calculation was successful in explaining a number of Doppler resolved observations for comets P/Halley and Hyakutake 1996B2 (Combi, 1989; Smyth et al., 1995; Combi and Cochran, 1997). Despite the fact that it is not clear that the mean rotational temperature extracted from the observed aperture-integrated spectrum should necessarily yield the same temperature as the mean value of the

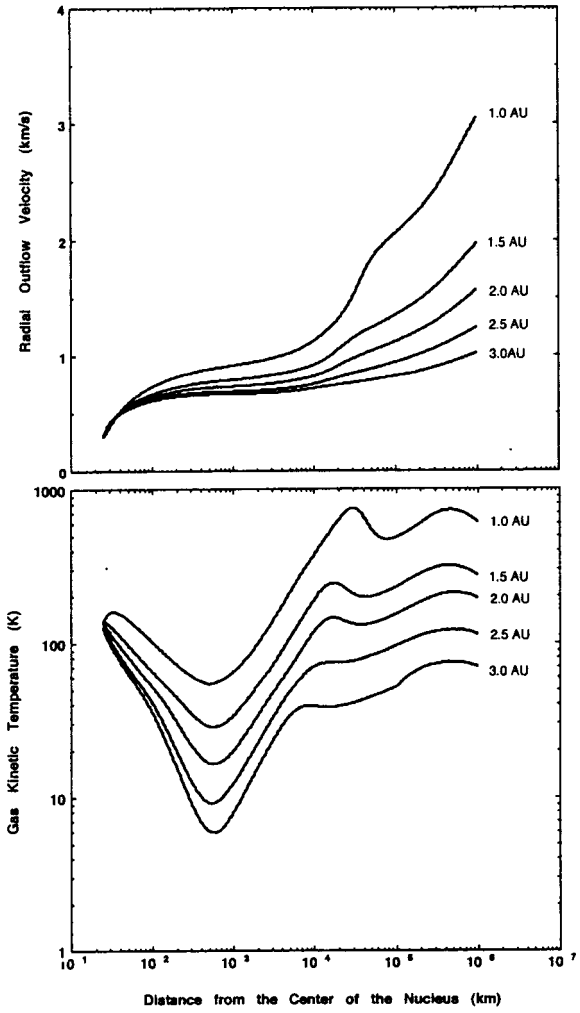

Figure 1. 1D-Spherical Hybrid Kinetic/Dusty-Gas Hydrodynamics. The results of 1D-spherical dusty-gas hydrodynamic model for comet Hale–Bopp where the photochemical heating rate is calculated by a kinetic Monte Carlo simulation.

gas kinetic temperature integrated over the same aperture, the agreement between temperatures and their variation between the observations and the simple model calculation is nonetheless quite good.

An independent confirmation of the model outflow speeds at large distances is found in a comparison with the analysis of the OH line profile observed with the Nançay radio telescope (HPBW of 3.5 by 19 arc mm) by Colom et al. (1997). Using a model which assumes an OH velocity of 1.05 km s^{-1}, water and OH lifetimes at 1 AU of 8.2×10^4 s and $1.1–1.6 \times 10^5$ s (the range coming from the heliocentric velocity dependence) they find mean water outflow velocities of 0.7 km s^{-1} for the

comet at 3 AU and 2.2 km s^{-1} at 0.93 AU. This is in excellent agreement with the outflow speeds at large distances from the comet at both heliocentric distances in the model calculation.

Measurements of gas species are typically interpreted using a model which adopts (by necessity) an outflow speed. The radial outflow speed for Hale–Bopp clearly varies with both distance from the nucleus and overall with heliocentric distance. Based on our calculations both variations can be expected to be much more pronounced than had been found for Halley (Combi, 1989) because of the enhanced photochemical heating efficiency in Hale–Bopp. Based on the comparison above with velocities and temperatures extracted from observations, we believe that the model velocities and temperatures shown here are reasonably representative of the conditions in comet Hale–Bopp. The velocities might be especially useful in the analysis of observations where the dynamical conditions in the coma are needed. These are given in Table II.

Observations of the coma of comet Hale–Bopp indicate that the ejection of dust into the coma is primarily, perhaps exclusively in the sun-ward direction (Rauer et al., 1997; Hayaard et al., 1997; Weaver et al., 1997). Near perihelion a well-developed system of dust haloes on the sunward side of the nucleus indicates that dust is ejected into a narrow jet from a primary active area when that area is illuminated by sunlight (Lederer et al., 1997; Larson et al., 1998). Gas seems also to be primarily produced from this active area, although it appears to remain active at a reduced level even when rotated into the apparent night side of the nucleus (Samarasinha et al., 1997–1999; Larson et al., 1998). It is clear then that although 1D spherical models are valuable for determining the nature of global average gas and dust dynamics, multidimensional models are necessary to understand many important attributes of comet Hale–Bopp.

We present here the results of a three-dimensional calculation for the dusty-gas dynamic flow in the vicinity of the nucleus for an active area superimposed on a uniform background. The calculation is performed on an unstructured multiscale Cartesian octree grid using adaptive mesh refinement. This octree structure is a hierarchical cell structure, based on multiple generations of cubic parent cells which can be split into 8 child cells (see DeZeeuw and Powell, 1992). The adaptive refinement of the mesh follows the gradients of the dynamical variables of the calculation and naturally results in the smallest cubes in regions where the flow gradients are the highest. Such a scheme makes optimal use of computer resources allowing problems with disparate scales and complex geometries to be modeled globally (i.e., a large simulation volume), while still retaining sufficient resolution for following small features locally, such as capturing shocks. The general numerical method has been applied to the MHD equations for the comet solar-wind inter-action (see Gombosi et al., 1996, 1997; Häberli et al., 1997a,b), and now to neutral dusty-gas flows without B-fields (Kabin et al., 1998).

Our method differs from a series of limited three-dimensional dusty-gas calculations by Crifo and coworkers (Crifo et al., 1995, 1997, 1998) in fundamentally

TABLE II

1D Spherical hybrid kinetic/hydrodynamic gas outflow velocities

	Heliocentric distance (AU)				
log d(km)	1.0	1.5	2.0	2.5	3.0
1.4	0.300	0.296	0.293	0.291	0.289
1.5	0.408	0.426	0.500	0.432	0.431
1.6	0.507	0.505	0.531	0.495	0.491
1.7	0.582	0.560	0.548	0.538	0.531
1.8	0 .641	0.603	0.585	0.570	0.561
1.9	0.689	0.636	0.613	0.595	0.585
2.0	0.728	0.664	0.636	0.616	0.604
2.1	0.760	0.687	0.656	0.632	0.619
2.2	0.787	0.706	0.672	0.646	0.631
2.3	0.810	0.722	0.686	0.656	0.640
2.4	0.830	0.737	0.697	0.664	0.647
2.5	0.848	0.749	0.706	0.671	0.652
2.6	0.863	0.759	0.713	0.675	0.655
2.7	0.876	0.767	0.719	0.678	0.657
2.8	0.887	0.774	0.723	0.680	0.659
2.9	0.898	0.780	0.727	0.682	0.660
3.0	0.908	0.786	0.730	0.684	0.662
3.1	0.919	0.793	0.734	0.687	0.663
3.2	0.930	0.799	0.738	0.689	0.665
3.3	0.943	0.807	0.743	0.692	0.667
3.4	0.956	0.816	0.748	0.696	0.669
3.5	0.972	0.826	0.755	0.700	0.672
3.6	0.991	0.837	0.764	0.706	0.677
3.7	1.013	0.851	0.773	0.714	0.682
3.8	1.040	0.867	0.785	0.723	0.690
3.9	1.076	0.886	0.798	0.735	0.700
4.0	1.119	0.911	0.816	0.749	0.711
4.1	1.170	0.943	0.838	0.766	0.722
4.2	1.232	0.986	0.868	0.785	0.732
4.3	1.307	1.042	0.904	0.804	0.742
4.4	1.401	1.100	0.940	0.823	0.752
4.5	1.528	1.150	0.972	0.840	0.761
4.6	1.681	1.193	1.004	0.858	0.771
4.7	1.815	1.230	1.029	0.876	0.782
4.8	1.910	1.266	1.056	0.895	0.793
4.9	1.983	1.303	1.109	0.914	0.804

TABLE II
Continued

5.0	2.048	1.341	1.112	0.934	0.816
5.1	2.112	1.382	1.142	0.955	0.827
5.2	2.181	1.426	1.174	0.978	0.840
5.3	2.255	1.475	1.210	1.003	0.856
5.4	2.338	1.530	1.249	1.030	0.874
5.5	2.433	1.591	1.292	1.059	0.894
5.6	2.543	1.659	1.339	1.091	0.915
5.7	2.666	1.732	1.390	1.124	0.938
5.8	2.796	1.809	1.445	1.160	0.963
5.9	2.926	1.887	1.503	1.198	0.989
6.0	3.050	1.964	1.562	1.237	1.016

d = distance from the center of the nucleus in km.

important ways. With their model they have already investigated a number of complicated emission conditions and geometries, including, weak and strong comets, multiple jets, many dust sizes, and non-spherical nuclei. Their calculation is performed on variable-sized, but fixed, spherical-polar grid. Because of the natural singularity in the spherical-polar grid at the pole, their solution is limited to regions away from the pole. Our method uses nested Cartesian cells, avoiding the geometrical singularity limitation and permitting fully global modeling adapting the cell structure to the calculation automatically, and with no spatial limitations.

Briefly the calculation solves the standard dusty-gas Euler equations for mass density, momentum and energy for a single-fluid gas and the equations for mass density and momentum of a number of dust particle sizes. For a detailed discussion see the review by Gombosi et al. (1986). The coupled system can be written in Cartesian coordinates as:

$$\frac{\partial \rho}{\partial t} + \nabla \cdot (\rho \mathbf{u}) = \frac{\delta \rho}{\delta t},$$

$$\rho \frac{\partial \mathbf{u}}{\partial t} + \rho(\mathbf{u} \cdot \nabla)\mathbf{u} + \nabla p = -\mathbf{F},$$

$$\frac{1}{\gamma - 1}\frac{\partial p}{\partial t} + \frac{1}{\gamma - 1}(\mathbf{u} \cdot \nabla)p + \frac{\gamma}{\gamma - 1}p(\nabla \cdot \mathbf{u}) = -Q,$$

$$\frac{\partial \rho_i}{\partial t} + \nabla \cdot (\rho_i \mathbf{v}_i) = \frac{\delta \rho_i}{\delta t}, \quad i = 1, \ldots, N,$$

$$\rho_i \frac{\partial \mathbf{v}_i}{\partial t} + \rho_i(\mathbf{v}_i \cdot \nabla)\mathbf{v}_i, \quad i = 1, \ldots, N,$$

where ρ is the gas mass density, $\mathbf{u}$ is the gas velocity, p is the gas pressure, $\mathbf{v}_i$ and ρ_i are the velocity and mass density for dust particles of radius a_i. The terms on the right hand sides of the equations are the various source terms. $\delta\rho/\delta t$ is the gas production source $\delta\rho_i/\delta t$ is the dust production source. F is the gas–dust drag force. Q is the dust–gas heat exchange rate. Then we can write the source terms as

$$\mathbf{F}_i = \frac{3\rho_i}{4a_i\rho_d} pC'_D \mathbf{s}_i,$$

$$\mathbf{F} = \sum_{i=1}^{N} \mathbf{F}_i,$$

$$Q = \frac{\gamma+1}{\gamma}\rho C_p u \sum_{i=1}^{N} (T_i^{\text{rec}} - T_i) St'_i,$$

$$\mathbf{s}_i = \frac{\mathbf{u}-\mathbf{v}_i}{\sqrt{2\frac{k_T}{m_0}}}.$$

Here C_p is the gas heat capacity at constant pressure and the rest of the coefficients can be defined under the assumption of diffusive reflection as:

$$C'_D = \frac{2\sqrt{\pi}}{3}\sqrt{\frac{T_i}{T}} + \frac{2s_i^2+1}{s_i^2\sqrt{\pi}}\mathrm{e}^{-s_i^2} + \frac{4s_i^4+4s_i^2-1}{2s_i^3}\mathrm{erf}(s_i),$$

$$T_i^{\text{rec}} = \left(1 + \frac{\gamma-1}{\gamma+1}s_i^2 R_i^1\right) T,$$

$$R'_i = \frac{\left(2s_i + \frac{1}{s_i}\right)\mathrm{e}^{-s_i^2}/\sqrt{\pi} + \left(2s_i^2 + 2 - \frac{1}{s_i^2}\right)\mathrm{erf}(s_i)}{s_i\mathrm{e}^{-s_i^2}/\sqrt{\pi} + \left(s_i^2 + \frac{1}{2}\right)\mathrm{erf}(s_i)},$$

$$St'_i = \frac{\mathrm{e}^{-s_i^2}}{8s_i\sqrt{\pi}} + \frac{1}{8}\left(1 + \frac{1}{2s_i^2}\right)\mathrm{erf}(s_i).$$

The dust bulk density, ρ_d, is the mass density of a particular dust particle. The gas temperature is T. The dust temperature, T_i, is constant for a particular dust particle size in equilibrium with solar radiation. C_p is the gas specific heat at constant pressure and the various other quantities are given assuming the standard free molecular conditions for gas–dust (Probstein, 1968 with minor corrections by Kitamura, 1986). These are s_i, the gas–dust relative Mach number, C'_D, the dust–gas drag coefficient, T_i^{rec}, the recovery temperature, R'_i, the heat transfer function, and St'_i the Stanton number. The equations are presented here in terms of the

primitive variables (density, velocity, and pressure); they are rewritten in terms of the conserved variables (mass, momentum, and energy) for the purpose of solving them numerically.

We first present here a calculation for a single concentrated gas/dust jet with uniform production over the rest of the nucleus. The nucleus is taken to be a sphere with radius of 28 km. Based on rough estimates relevant for comet Hale–Bopp at 1 AU, we have set 30% of the gas and dust production to come from a single active area with a Gaussian in angle having a width of 10° (half-angle), and the remaining 70% spread uniformly over the nucleus. The total gas production rate of 10^{31} s^{-1} with a mean molecular mass of 20 amu is adopted. Six sizes of dust particles with radii of 0.1, 1, 10, 100, 1000, and 10000 μm (the latter three corresponding to 0.1,1 and 10 mm) are adopted with a dust-to-gas mass ratio of 5 (Schleicher et al., 1997) and a number distribution varying as $a^{-3.5}$, where a is the particle radius. The precise value of the dust-to-gas mass ratios depends critically on the extension of the population to very large particles, which contain most of the mass, and the functional form of the size distribution which is not well-specified. For example, essentially the same distribution of small particles for comet Halley yielded total dust-to-gas mass ratios varying from 0.3 (Gombosi, 1986) to greater than 1 (Crifo, 1991). The actual difference was only in the extension of the distribution to the very large particles (cm-sized) by Crifo, which affect neither the gas dynamics, nor contribute to ground-based observations of dust continuum.

For the model calculations shown here the entire simulation box extended to ± 50 times the nucleus radius (R_n), or to 1400 km from the nucleus. A total of 220,000 cells were included in the simulation and the cells ranged in size from 0.78–10R_n. The adaptive mesh structure is shown for the full simulation box and for a magnified region near the nucleus in Figure 2. As in the models of Crifo and co-workers each dust size is a separate fluid, however in our case the full multi-fluid calculation is carried out in the whole simulation volume. The full multifluid calculations of Crifo and co-workers which include many more dust sizes (up to 44 logarithmically spaced sizes) are typically carried out in a restricted volume near the nucleus, and are extended to large distances outside the subsonic region using a steady-state expansion calculation. In our full calculation each dust size introduces four additional equations and unknowns to be solved in every cell.

There are a number of important and interesting results from our dusty-gas calculation. Figures 3a,b show color contour plots of the number density of the gas with superimposed velocity streamlines and the gas speed. Note that the gas flow lines originating from the active area expands tangentially near the nucleus but that by a several R_n the flow is essentially radial and the asymmetry due to the active area is frozen-in. Figures 4a,b and 5a,b show similar pairs of plots for two of the sizes of dust with radii of 1 μm and 1 mm. In all cases the color table for the speed plots is the same. Colors for the density are relative because of the large differences in dust bulk mass density from size to size and compared with the gas. We selected these two particular dust sizes because both the density and speed

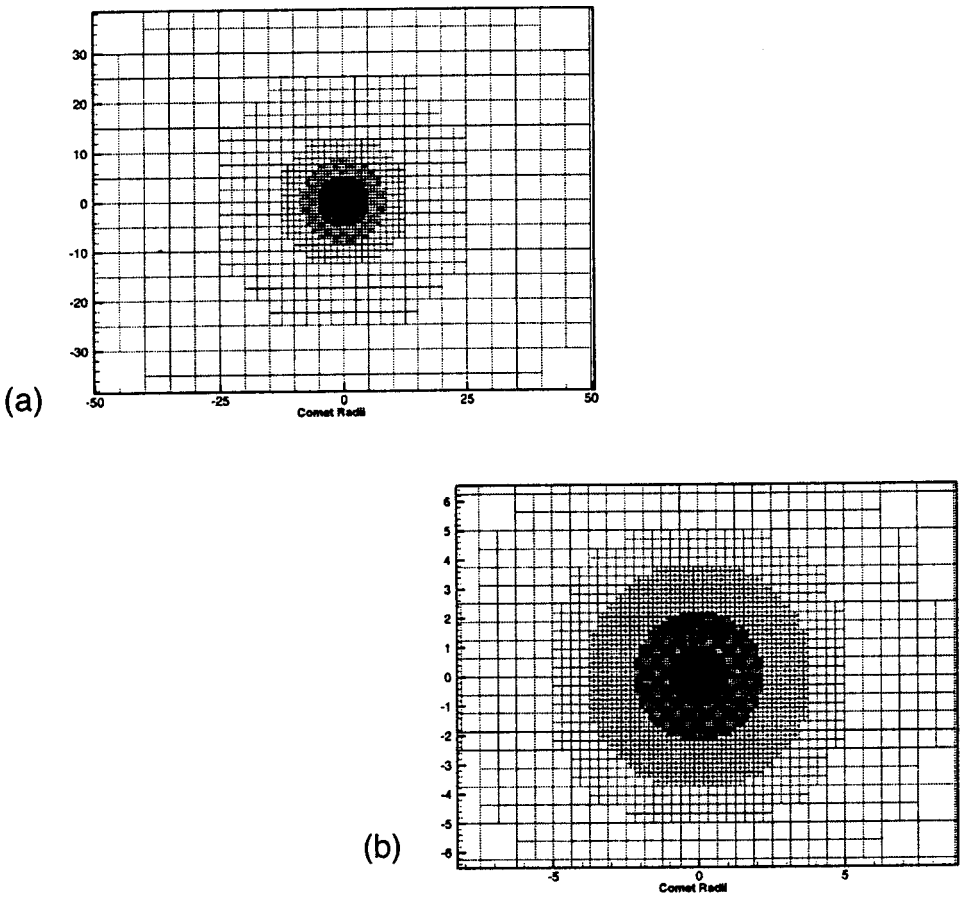

Figure 2. Two views of adaptive mesh for dust–gas jet calculation. Above in (a) the whole simulation volume is shown extending to 50 nucleus radii (1400 km) from the nucleus. Below in (b) the cell structure around the nucleus is shown, where the nucleus corresponds to the black circle at the center.

variations are typical for the nearby dust sizes. The plots for the 1 μm particles are very similar to those for the 0.1 and 10 μm particles. Those for the 1 mm particles are similar to those for the 0.1 and 10 mm particles, although the speeds of course are somewhat larger and smaller, respectively, for the two groups. For all dust sizes the dust jet remains more concentrated over the active area and the gas squirts laterally to the side of the dust jet, making the gas distribution more uniform over the day-side hemisphere than the dust. This is not unexpected.

The dust velocities for the small dust sizes (0.1, 1, and 10 mm) follow the gas flow quite closely. Because of the dust mass loading, the gas and small-dust speeds are slowest in the middle of the dust jet and fastest throughout the uniform background. Owing to the large gas densities the smaller dust sizes follow the gas flow very closely everywhere, and only the larger dust sizes show the conical type structure which has been seen even in the early 2D-axisymmetric dusty-gas jet

modeling (Kitamura, 1986; Körösmezey and Gombosi, 1990). Furthermore, the larger dust sizes achieve the highest speeds in the jet (i.e., to the left in Figure 5b), where the gas densities are the highest, and somewhat lower speeds away from the jet (i.e., to the left in Figure 5b), the opposite behavior of the small particles.

The most important implications from the model calculations result from the overall large dust speeds of all particles, compared with past calculations of moderately bright, Halley-class, comets. All of the particles in the optical size range, i.e., those that make the dominant contribution to optical CCD imaging of the dust coma, and of course smaller particles, are accelerated to $\sim$90% or more of the gas velocity. There is only a small range in speeds. Even the 10 μm particles are accelerated to $\sim$75% of the gas speed. The uniform speeds of particles in the optical size range may be responsible for the sharpness of the observed dust jets in Hale–Bopp and for the rough spatial coincidence (or at least roughly similar spiral pitch angles) of the spiral dust jets and gas jets in the CCD-images (Larson et al., 1998; Lederer et al., 1997; Samarasinha et al., 1997–1999). In Halley, the small grains suggested to be the source of the gas jets (sub-μm) were accelerated to nearly the gas velocity, but the larger optical-size grains (μm sized) were not. The combination of different outflow speeds with nucleus rotation produced a velocity sorting effect between gas (CN) and dust jets (Samarasinha, private communication). In Hale–Bopp near perihelion, our calculation shows that all the optical and smaller particles are accelerated to nearly the gas speed. Therefore, there should be little velocity-sorting between optical and smaller particles, resulting in sharp dust jets, and gas jets following the same spiral arcs as the dust jets. We have also run a model with 85% of the gas production and all of the dust production coming from one active area, and the resulting large dust velocities for optical-sized particles are similar (see below).

Only the largest particles show the typical fall-off velocity with increasing particle size, however, the velocities are still much larger than the usual published values that are based on comets with much lower gas production rates (Crifo, 1991; Gombosi et al., 1986). This may have important consequences on the estimate of total dust-to-gas mass ratios extracted from long-wavelength observations which are sensitive to detecting most of the dust mass that is present in mm-sized particles (Senay et al., 1998). In Table III we show values of the gas and dust particle velocities at different angular locations compared with the jet near the outer portion of the simulation box at a distance of 1300 km from the center of the nucleus.

Only preliminary reduction and analyses have been performed on the data needed to properly characterize the realistic balance between the separate components of gas and dust in an active jet and in a uniform background. The two cases we have examined, one with 30% of the production in the jet and one with 85% of the production in the jet, yield very similar large dust particle speeds. Therefore, the large dust speeds can be used in the next iteration of the process of trying to understand the temporal and geometric aspects of rotating dust and gas jets in the coma from the observations. They should also be used in the interpretation of long

TABLE III
Gas and dust terminal speeds in a 3D dust–gas jet

Species	Terminal speeds in m s^{-1}			
	In jet	45°	90°	135–180°
Gas	718	734	748	810
0.1 μm	698	718	727	795
1.0 μm	647	668	669	741
10 μm	549	556	555	603
0.1 mm	394	370	370	355
1.0 mm	212	182	182	148
10 mm	84	72	73	48

wavelength observations which detect mainly the large mm-sized particles which are the dominant contributors to the global dust mass production rate.

For comparison with the first model results shown in Figures 3–5, Figures 6a,b show the gas number density and dust bulk mass density for the 1-μm optical-sized particles in the vicinity of the nucleus in the case of a strong jet where 85% of the gas production and 100% of the dust production is in the jet and only 15% of the gas production is distributed uniformly around the nucleus. For this more confined distribution of material at the surface of the nucleus the dust jet remains more focused but the gas distribution broadens, expanding to 2 to 3 times its original Gaussian width. Some evidence from the observed images indicates that the observed jets may be narrower than even this model where 85% of the production is in the jet. This could indicate a role for some kind of collimation due to the spatial topology of the surface, which is not in our current model. Such collimation could be caused by the active area that produces the jet being recessed into the surface as in a crevasse or a crater. The effects of surface topology and local solar insolation which has possible influence on the strength and appearance of gas and dust jets have begun to be addressed by Crifo et al. (1998).

Boice et al. (1998) have also recently presented results of a 1D-spherical dusty coma model of comet Hale–Bopp at several heliocentric distances which includes the surface layer as part of the calculation. Their calculation accounts for gas emission from the surface, from transport through a porous surface layer, and from release of gas from dust in the coma. Separate fluids are included for electrons, heavy neutral gas, fast hydrogen, and dust.

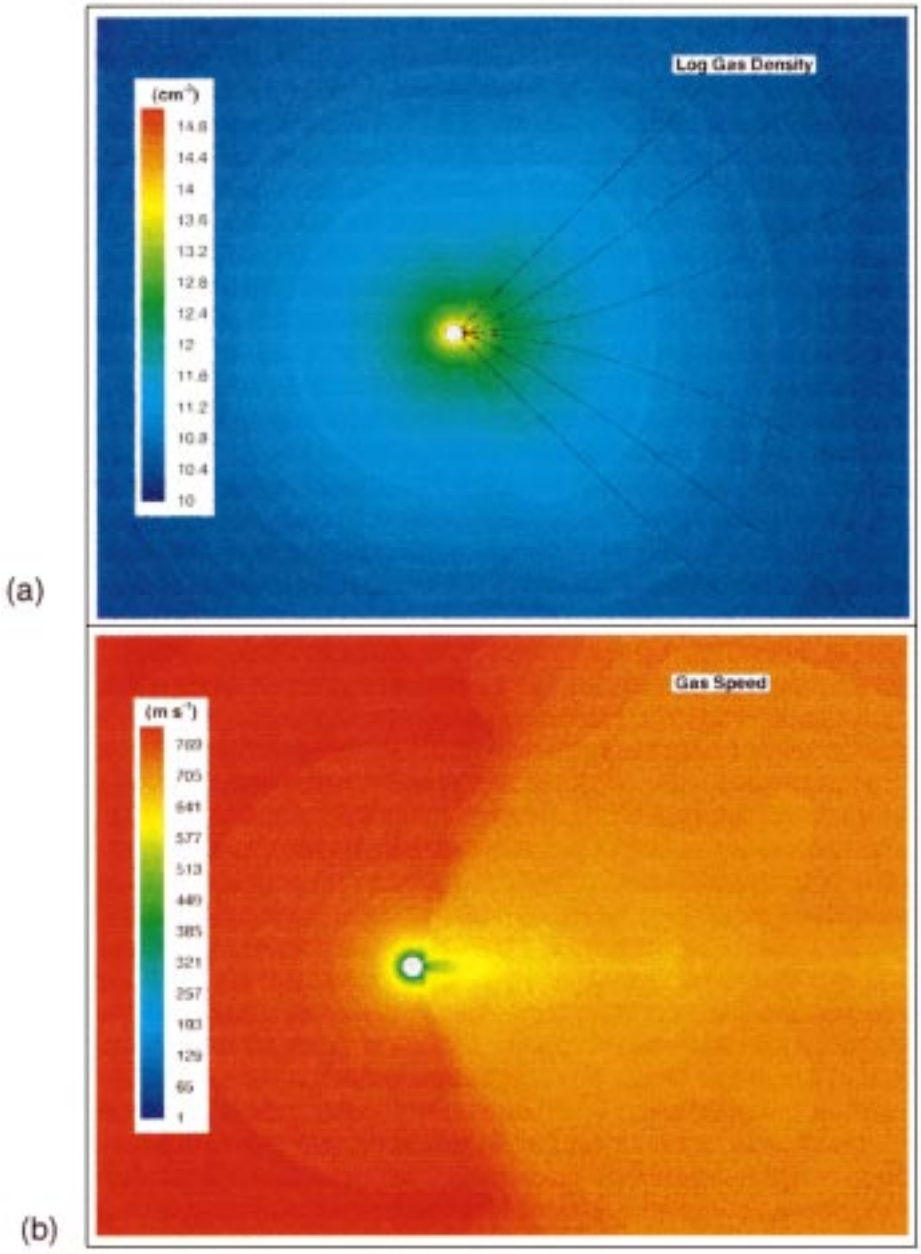

Figure 3. 3D Dusty-Gasdynamic model of a dust–gas jet. Shown are (a) the number density of gas and (b) the speed of the gas. The calculation corresponds to comet Hale–Bopp at ∼1 AU. The jet is directed toward the right.

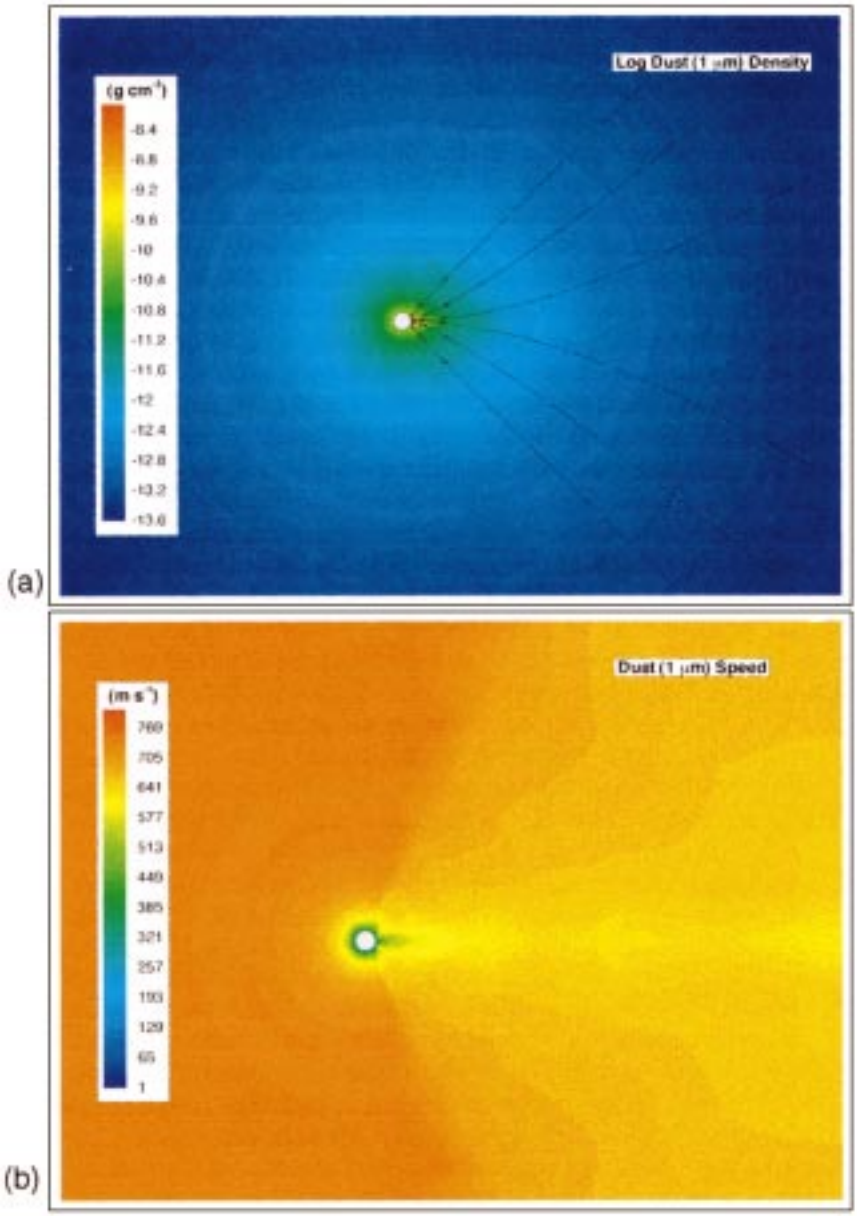

Figure 4. 3D Dusty-Gasdynamic model of a dust–gas jet. Shown are (a) the bulk mass density and (b) the speed for the μm dust particles. The calculation corresponds to comet Hale–Bopp at $\sim$1 AU. The jet is directed toward the right.

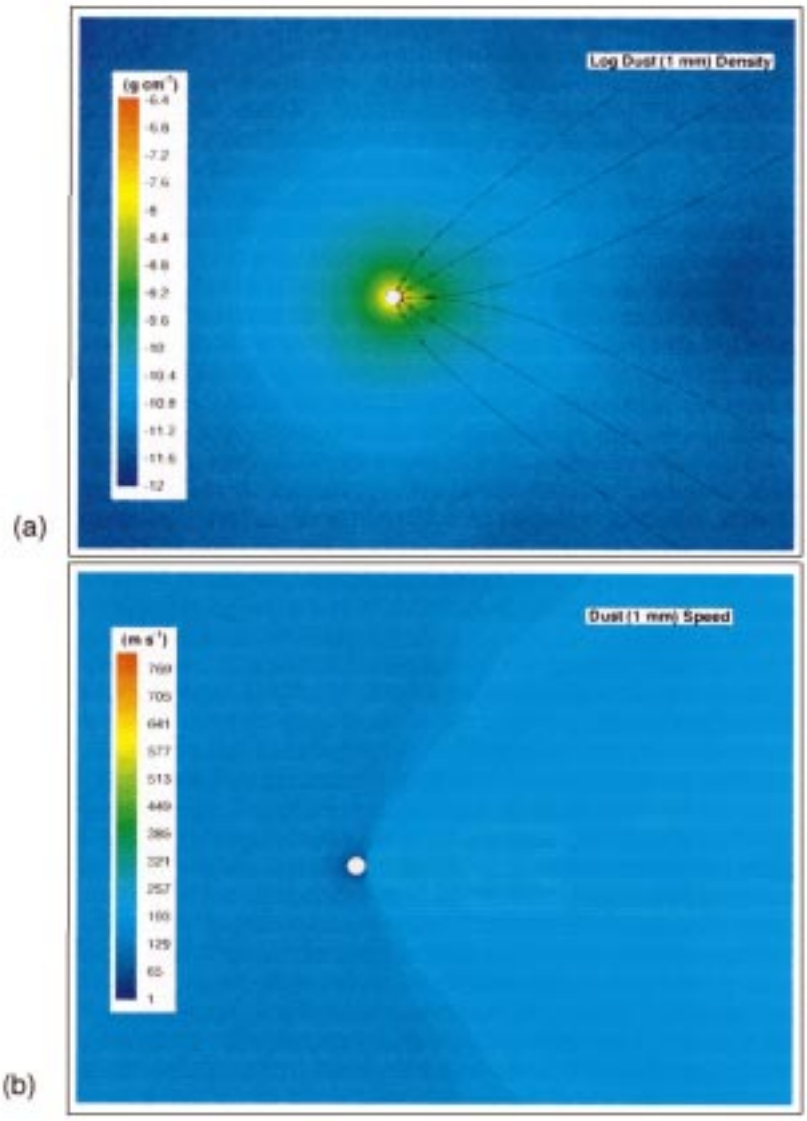

Figure 5. 3D Dusty-Gasdynamic model of a dust–gas jet. Shown are (a) the bulk mass density and (b) the speed for the 1 mm dust particles. The calculation corresponds to comet Hale–Bopp at ∼1 AU. The jet is directed toward the right.

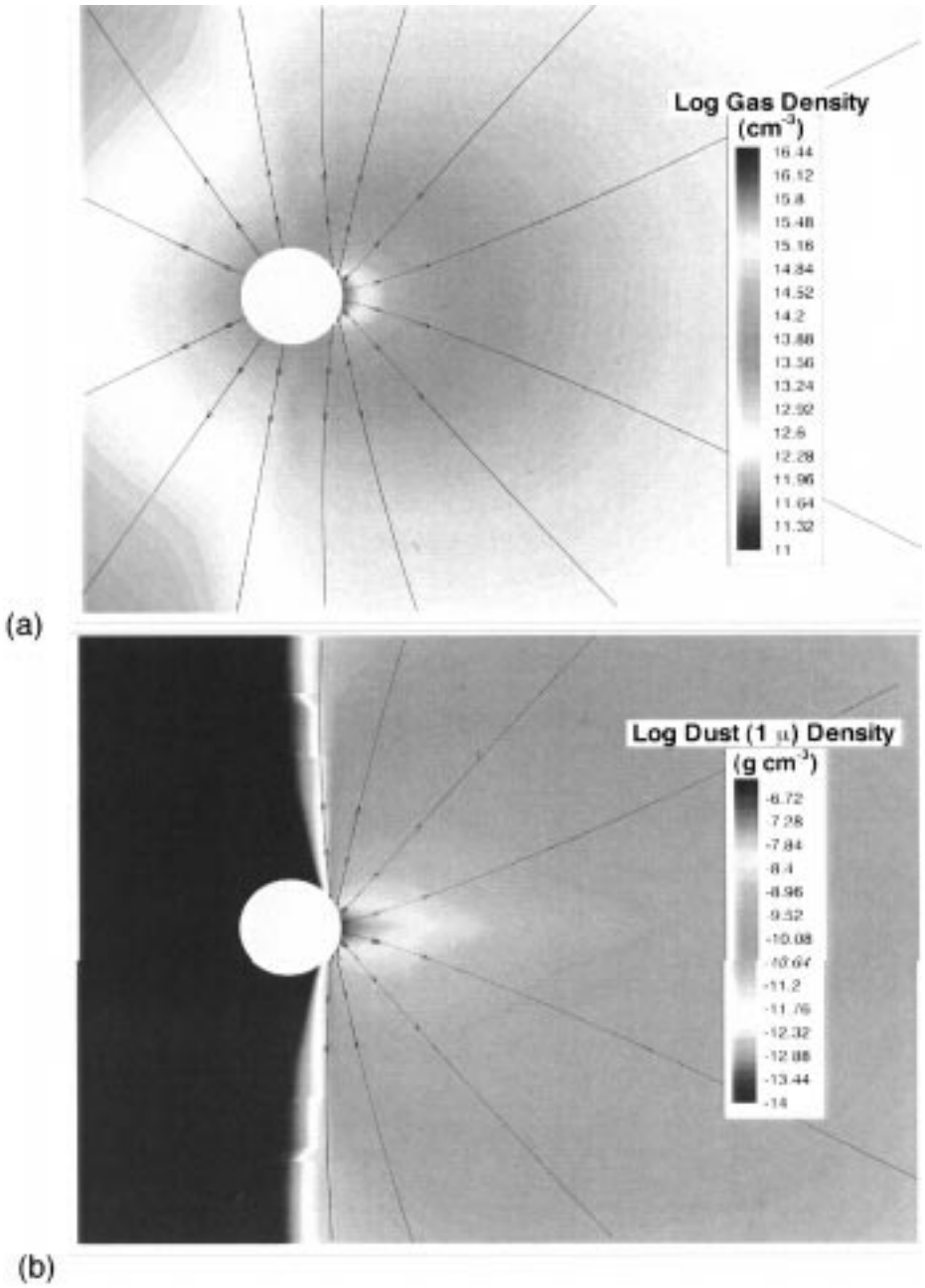

Figure 6. 3D Dusty-Gasdynamic model of a strong dust–gas jet. Shown are (a) the number density of the gas and (b) the bulk mass density for optical 1 μm particles in the vicinity of a strong jet, directed toward the right.

3. Evidence from Observations

3.1. Extended sources of gas

The discovery of an extended source of formaldehyde (H_2CO) in comet P/Halley by Eberhardt et al. (1987) using data from the Neutral Gas Mass spectrometer on the Giotto spacecraft provided conclusive evidence of a substantial source of a gas species from unseen parent grains. There was not a sufficient amount of another heavier parent molecule to account for H_2CO which was present at the $\sim$7% level compared with water. That H_2CO is produced by an extended source in comet Hale–Bopp has also been suggested by Womack et al. (1997) and Wink et al. (1997). Radio observations of HNC by Biver et al. (1997a) and mm-wavelength observations of CH_3OH by Womack et al. (1997) indicate that these species are also produced by an extended source. However, whether they are produced by grains or molecules (e.g., by photodissociation) is not yet known. In addition, the H_2CO itself was also found to serve as an important extended source for a substantial fraction of cometary CO (Meier et al., 1993; Samarasinha and Belton, 1993). This has since been seen in infrared observations of a number of subsequent comets including most recently Hyakutake and Hale–Bopp (DiSanti et al. 1998). From radio observations of the OH radical in Hale–Bopp, Colom et al. (1997) report evidence for water sublimation from grains.

3.2. Dust and gas jets, haloes and shells

One of the most interesting aspects of the early analysis of observations of Hale–Bopp is the dominance of gas jet activity. Shortly after discovery at nearly 7 AU it was found that CO, probably the dominant species at that time, was being produced in a narrow, well-focused, day-side jet (Jewitt et al., 1996). Subsequently dust jets in various configurations were seen to dominate continuum images (Kidger et al., 1996; Weaver et al., 1997). Near perihelion in addition to the well-developed day-side dust haloes, which were apparent to anyone looking at the comet through even an amateur telescope, narrow-band CCD imaging showed a set of gas jets/haloes. The dust sources were only substantially active on the day side of the nucleus. This created a pattern made by one or more spiral jets which were not visible on the night side. The gas jets, however, continued activity on the night side, but at reduced level. Therefore, the gas jet spiral pattern was generally more continuous.

The CN radical, along with C_2, was one of the earliest spectroscopic detections made in comets (Huggins, 1882). Coming from the presumption that CN was produced by the photodissociation of some stable parent molecule, early studies (Potter and DelDuca, 1964; Jackson, 1976) lead to the suggestion of various candidate species (HCN, C_2N_2, CH_3CN, HC_3N, etc.). The study of a large sample of both radial spatial profiles of CN (Combi and Delsemme, 1980) and sunward and antisunward profiles distorted by radiation pressure acceleration (Combi, 1980) lead them to conclude that the observational evidence was consistent with the

production of CN by the photodissociation of HCN which had been discovered by radio emission (Huebner et al., 1974). However, their results were based on modeling the parent molecule outflow speed using the a heliocentric distance dependent velocity law of $0.58r^{-0.6}$ km s^{-1} (Delsemme, 1982) which is now known to be too small. Later comparisons of production rates from radio observations of HCN and optical observations of CN (Bockelée-Morvan and Crovisier, 1985) showed that, although for some comets the production rates were roughly equivalent, for others the CN production rate was too large. This indicated multiple sources for CN with different relative compositions, varying from comet to comet.

The discovery of jets of CN in comet P/Halley by A'Hearn et al. (1986) lead them to the conclusion that the CN seen in the jets (at least) was produced from very small CHON (organic particulates rich in compounds containing carbon, hydrogen, oxygen, and nitrogen) grains. They reasoned that only a grain source would remain tightly entrained in the collimated flow. Although it was clear that most gas species and dust were produced from the same major active areas on the surface of the rotating nucleus (Millis and Schleicher, 1986), the non-coincidence of CN and dust jets was explained as a velocity sorting according to grain size. The dust continuum was dominated by micron-sized grains which are accelerated only to some fraction (0.5 or less) of the gas velocity (Gombosi et al., 1986), whereas the CN in the jets was produced by very small CHON grains, which are accelerated to nearly the gas speed. Combi (1987), on the other hand, suggested that a localized source of parent molecules might remain collimated enough without the requirement to invoke grains. Parent molecules obviously travel at the gas speed so the non-spatial coincidence would be same whether produced from molecules or sub-micron CHON grains. A subsequent analysis of the CN-jet images by Klavetter and A'Hearn (1994) showed different radial distributions for CN within the jet compared to the CN between the jets, pointing again toward a CN-jet source (grains) with a length scale of $\sim$8000 km, similar to that observed for H_2CO. In addition to CN and C_2 jets (Schulz and A'Hearn, 1995), Cosmovici et al. (1988) also reported jets in images of C_3, as well as in a combination image of [OI] plus NH_2 emissions in comet P/Halley.

For comet Hale–Bopp pre-perihelion observations of HCN (Biver et al., 1997a) and CN (Schleicher et al., 1997; Rauer et al., 1997) indicate there is a rough equivalence of the HCN to CN production rate for heliocentric distances larger than about 4 AU. By 3 AU the relative CN production rate increases over HCN by about 60%, and although the published data are incomplete at the time of this writing, indications are that the ratio is approaching 2 near perihelion. Such a behavior is consistent with the gradual activation of a second source of CN at smaller heliocentric distances. Rauer et al. (1997) suggest possible sources in grains which might be activated by 3 AU, or additional parent molecules (CH_3CN and HCN). Fitzsimmons and Cartwright (1996) and Wagner and Schleicher (1997) suggest that the appearance of CN spectroscopically at greater than 6 AU from the sun points to the same mechanism for at least a large fraction of the CN seen at small heliocentric

distances. Therefore, a reasonably consistent picture emerges for a combination of sources. The major one is probably the photodissociation of some set of more volatile parent molecule species including HCN which are active at large heliocentric distances. Then at smaller distances (3 AU) an additional source becomes activated which could be either less volatile parent molecules, small vaporizing grains, or some combination. The variation of the ratios of the various sources from comet to comet, with time (heliocentric distance), and possibly with location on the nucleus, could explain many of the difficulties in tying together a simpler consistent picture with HCN alone (Bockelée-Morvan and Crovisier, 1985).

Regarding the identity of other photodissociation parents for CN, Festou et al. (1998) are suggesting C_2N_2, which has been already on candidate lists for a long time. They find that the a combination of a lifetime of 3.5×10^4 seconds at 1 AU and a CN velocity of 1–2 km s^{-1} can explain the observed characteristics of production scale length and the Doppler-broadened velocity profiles. However, caution must be taken that model analysis must account properly for the expected large parent molecule outflow velocities (2 km s^{-1} at 10^5 km) and collisional quenching of the ejection velocity received by daughter radicals upon dissociation of their parents. These attributes of comet Hale–Bopp have been discussed above.

Lederer et al. (1997) have reported gas jets in all of the major visible neutral species, CN, C_2, C_3, NH, and (most importantly) OH during the two-month period surrounding perihelion. Wink et al. (1997) have presented Doppler-resolved radio observations during the same period of CO, HCN, CS, and H_2CO, which indicate production these species into localized jets rotating with the nucleus. The CO jet is active on both the day and the night side and appears to be located at the equator. The average line-of-sight velocity of CO varies periodically with the 11.3-hour rotation period of the nucleus and has an amplitude of about 0.2 km s^{-1} This is not necessarily indicative of the ejection speed of gas from the jet, but the integrated deviation from a stationary mean composed of the coma average with the velocity dispersion of the jet projected along the line of sight. Wink et al. find that the HCN emission comes from the same location as CO but is weakened in the night side. The CS emission changes in a similar manner but appears to come from an active area in a different location in the northern hemisphere. The H_2CO emission appears in phase with CS but is systematically more blue-shifted. Because H_2CO is not a parent species (likely produced by grains), the extra velocity shift may not be surprising.

Larson and Hergenrother (1998) have presented reduced (i.e., continuum subtracted) CN images and dust continuum images. These show that dust jets and CN jets generally follow the same spiral geometry with nucleus rotation. Taken at face value this means that the velocity of the CN source and the velocity of the dust is about the same. As mentioned already this is in contrast to the case for Halley (A'Hearn et al., 1986) where the gas jet and dust jet had different spiral pitch angles, indicating different velocities. One interesting exception to the jet coincidence was

a CN-only jet (or possibly more accurately, a gas-only jet) reported by Larson and Hergenrother.

Samarasinha et al. (1997–1999) have presented a preliminary model for the CN gas jet which reproduces some of the basic features of their own CN images. Their images are otherwise similar to the above-mentioned data from Lederer et al. and Larson et al. Although the detailed appearances of gas and dust jets change with activity and rotation from day to day during this period, the general existence and appearance of dayside dust spirals and dayside and nightside gas spirals were consistent. Their model has a single active region as the source of the CN jet which continues activity on the night side of the nucleus at about 10% of the level on the day side. Taken at face value this might be consistent with the HCN observations of Wink et al. (1997) mentioned above, perhaps suggesting a connection between HCN jets and CN jets, at least in comet Hale–Bopp. If the dust jet activity had continued at a similar level into the night side, it would be very obvious in continuum images. Therefore, it is apparent that the dust jet activity on the night side is reduced to well below the 10% level. This is consistent with the appearance of dust jets in other comets, even Comet Hyakutake (1996 B2), which showed well-developed day-side dust jets but fairly uniform (spherical) emission of gas species (CN and OH) from the vicinity of the nucleus (Harris et al., 1997).

Based on the dusty-gas modeling results presented in the previous section of this paper, it is clear that the dust–gas dynamic regime for comet Hale–Bopp, especially with the dominance of local active region(s), is very different from the more typical active comet, e.g., P/Halley, and C/Hyakutake (1996 B2). Even fairly large particles (10 μm) in the dust–gas jet will be accelerated to a large fraction of the gas velocity. This means that it is quite natural for the gas and dust jets to be spatially similar in Hale–Bopp, but not so in P/Halley.

Perhaps the more interesting question raised by the existence of gas jets of CN, C_2, C_3, NH, OH (implying H_2O), CO, CS, and H_2CO, and the similar day-night behavior of CN and HCN jets regards the original conclusion by A'Hearn et al. (1986) that the CN in the CN jets of comet P/Halley were produced necessarily from CHON grains. As mentioned above, Combi (1987) had suggested that the parent of the CN in the jets might have just been a local enhancement of a parent molecule, i.e., gas emitted by the local active area which remains focused in a jet. A parent molecule would of course move with local gas speed, just as the small sub-micron grains invoked to explain the CN jets. Dusty-gas hydrodynamic models for localized active regions (Kitamura, 1986; Körösmezey and Gombosi, 1990; Crifo et al., 1995) have always indicated that radial expansion near the nucleus is rapid and that any jet asymmetry frozen-in by a few nucleus-radii would be maintained to considerable distances. Therefore, the general spherical symmetry of the gas coma in some comets, is probably not due to a simple isotropization from the physics of the inner coma flow expansion from day-side active areas. Either distributed production of gas species over the surface or significant extended production of gas from volatile grains away from the nucleus is required. Comet Hyakutake

(1996 B2) is an example of a comet with active dayside dust jet production but nearly spherical gas (CN and OH) distribution. There is also direct and indirect evidence for significant gas production from icy particles away from the nucleus (Harris et al., 1997).

3.3. THE CASE FOR C_2

It has been noticed for a long time that the radial distribution of C_2 radicals in comets is unusual compared with most other daughter species (e.g., CN, C_3, NH_2, etc.) whose distributions can all be reproduced by a photochemical model that accounts for one generation of exponential decay from a parent molecule. Delsemme and Miller (1971) suggested that the radial distribution could be explained if C_2 radicals were trapped in clathrate-hydrate icy grains which were liberated from the nucleus similarly to refractory dust particles, dragged away by the out-flowing gas, and subsequently vaporized releasing the free C_2 radicals. They presented a mathematical icy grain halo model, which could be fitted to an observed C_2 profile, as an alternative to the photochemical Haser model, which fit poorly. A number of subsequent investigators who published spatial profiles of C_2, sometimes noted the same problem and suggested either that C_2 was produced from grains, or it was produced as a grand daughter species from a primary parent molecule.

Despite the difficulty, observed C_2 profiles (Cochran, 1985; Combi and Delsemme, 1986; Wyckoff et al., 1988; Fink et al., 1991; Schulz et al., 1993; Cochran and Trout, 1994) and the extraction of production rates for all species from standard cometary aperture photometry (A'Hearn et al., 1995) have typically been analyzed using a standard 2-generation Haser model. In recent years more and more analyses of observations of OH (e.g., Weaver et al., 1997; Budzien et al., 1994; Cochran and Schleicher, 1993) and CN (Schulz et al. 1993a,b, 1994) have been performed using a vectorial model. Such is not normally the case for C_2. The best-fit Haser scale lengths have generally depended upon the spatial coverage of the data. Parent and daughter scales lengths which are more nearly equal are found if the data cover distances close to the nucleus (Wyckoff et al., 1988: Fink et al., 1993; Schulz et al., 1993). Parent and daughter scale lengths in the ratio of ∼6–8 to 1 are found if the data cover distances farther from the nucleus (Cochran, 1985; Combi and Delsemme, 1986).

By scaling a set of radial profiles of C_2 in comet P/Halley which assumed their length scale follow an $r^{1.5}$ variation (r = heliocentric distance) O'Dell et al. (1988) produced a single average C_2 profile covering several orders of magnitude in normalized distance both very close to and very far away from the nucleus. They used a 3-generation version of a Haser-type photochemical model with a sequence of three scale lengths in the ratio of $1:5:50$ corresponding to parent, daughter, and C_2 as granddaughter to account for the shape of the composite profile. The recent discovery of acetylene (C_2H_2) in comet Hyakutake and subsequent measurement in comet Hale–Bopp, provides a prime candidate, present at the ∼1% level, for the 3-

generation chain (C_2H_2 to C_2H to C_2). This particular chain has been suggested for many years (Jackson, 1976; Yamamoto, 1981; see the review by Jackson, 1991).

However, this 3-generation model, like the standard Haser model, ignores the existence of expected excess energy at each photodissociation which has been properly included in the vectorial model (Festou, 1981) and otherwise similar Monte Carlo models (Combi and Delsemme, 1980). In a more recent spatial profile study for individual profiles in comet P/Halley, Combi and Fink (1997) examined both 3-generation models which included daughter species ejection velocity and a new version of a grain source model that modifies some properties of the older icy grain halo model (Delsemme and Miller, 1971) to be appropriate for CHON grains which have been suggested as sources for CN and C_2 jets (A'Hearn et al., 1986; Klavetter and A'Hearn, 1994; Schulz and A'Hearn, 1995). They found that if the 3-generation model is correct then there are strict limits to the total ejection velocities for both dissociations taken together of <0.5 km s^{-1}. In addition, they also found that a CHON grain halo could explain the radial distribution for a halo size of about 88,000 km at a heliocentric distance of 1 AU. This is the expected radius for velocity and lifetime of submicron ($\sim$0.2 μm) CHON grains (Lamy and Perrin, 1987) if they behave as laboratory tholins (Khare et al., 1984).

Another approach into the question of the source of C_2 radicals has been found in comparing the spatial dependence of the (1-0) to the (0-0) Swan bands by Roussellot, Laffont and co-workers. Roussellot et al. (1994) suggested that their observed variation of C_2 (0-0) and (1-0) in comet P/Halley indicates production of vibrationally cool C_2 from the nucleus, presumably from the photodissociation of some parent molecule and hot C_2 in a spatially extended region and in the vicinity of observed jets, which is consistent with production from hot grains. More recent observations of comet Hyakutake (C/1996 B2) by Laffont et al. (1997) yield similar results indicating the production of cool C_2 near the nucleus but the production of high excitation temperature C_2 in the region associated with the antisunward-drifting condensations, clumps or clusters. Laffont et al. (1998) are presenting the results of similar observations and analyses in comet Hale–Bopp at this conference.

In analysis of spatially-resolved (1D) spectroscopic observations of Hale–Bopp, Korsun et al. (1997) find similarities between the distributions of C_2 and dust continuum not shared by other gaseous species. They find that the other gaseous species (NH_2 and CN) are roughly symmetric (sunward–antisunward) with respect to the nucleus, but that C_2 is asymmetric with a sunward preference similar to the dust continuum. They reason that this is due to production of some of the C_2 from the dust. Sekiguchi et al. (1997) also report more specifically, based on observations of Hyakutake and Hale–Bopp that most C_2 is produced from C_2H_2, but that some C_2 is produced from dust.

3.4. DUST FADING AND FRAGMENTATION

A radial profile of column abundance (or brightness in the optically thin limit) varying as the inverse of the projected distance, ρ, is found for a simple constant point source expanding at a constant velocity. This is the simplest picture of dust production in comets. Even in the realistic case where solar radiation pressure is important, the radial profile in the direction away from the sun, as projected on the sky plane, is still found to vary as the inverse of the projected distance (Wallace and Miller, 1958). Evidence for the departure from a $1/\rho$ distribution were reported by Jewitt and Meech (1987) and Jewitt and Luu (1989) from analyses of the radial profiles of dust continuum observations in comets. In spite of a technical error in their mathematical model discussed by Combi (1994), the finding by Baum et al. (1992) of what they called dust fading on scales of $\sim 10^4$–10^5 km in some comets, but not all, appears to remain valid. They found departures from the simple $1/\rho$ distribution which could be interpreted as a loss of particles with increasing distance from the nucleus. Preliminary indications from observations of comet Hale–Bopp (Schleicher, private communication) are that grain fading does not occur on this spatial scale.

On the other hand, there is evidence that grain fragmentation in the very innermost comae of active comets may be quite important. The brightness profiles of dust continuum determined with the Giotto Halley Multicolor Camera experiment (Keller et al., 1986) within a few tens of km of the nucleus of comet P/Halley flattened considerably. This occurred at distances where dust particles could still be accelerated by outflowing gas, and one might expect to have observed the brightness profile become more steep not less. The fragmentation of particles has the opposite effect from fading on the radial profile (Thomas and Keller, 1990; Konno et al., 1993). As particles break apart, the total surface area of all the small particles is larger than those of the original large particles, in the absence of evaporative loss. This increases the total scattering cross section and thus increases the brightness, relative to the base-line $1/\rho$ with increasing distance.

In addition to the Halley Giotto images, there is evidence for fragmentation in the analysis of ground-based dust coma and tail images. In an analysis of dust tail images of comet Austin (1990 V) with their inverse Monte Carlo model, Fulle et al. (1993) found that a considerable spread of initial velocities, the so-called terminal velocity, was required for particles having any particular size. This is contrary to the standard Finson–Probstein (1968) dusty-gas dynamics picture which implicitly assumes non-fragmenting particles, and where particles of a certain size and bulk density are accelerated by the gas flow to a particular single velocity, i.e., the velocity distribution for a certain size particle is a delta function. Combi (1994), in order to reproduce ground-based dust coma images of comet Halley using a Finson–Probstein-type Monte Carlo simulation, introduced a heuristic dust-fragmentation function, which assumed that particles started with some velocity given by dusty-gas dynamics and then fragmented into a population of smaller particles. More

recent modeling by Fulle et al. (1997) for Hyakutake (1996 B2) similarly requires a velocity dispersion for each particle size, implying that particle fragmentation is important within, and perhaps just outside, the dusty-gas acceleration region (typically a couple of hundred km).

Based on the modeling discussed in the previous section of this paper, it appears that for comet Hale–Bopp a wide range of particle sizes will be accelerated to nearly the gas velocity, especially within the concentrated jets. The more uniform velocities for the particles in the 0.1 to 10 μm range, which typically dominate the observed visible dust coma, will probably make the analysis of dust coma and tail images a less sensitive indicator of particle fragmentation than other recent and more moderate comets. All particles regardless of whether they were primary parent particles, or fragments of them, will all be accelerated to nearly the gas velocity and thus will not have much dispersion in velocity.

4. Summary

We have presented a review of the state of knowledge regarding issues of dust–gas interrelations in comets, especially as it relates to comet Hale–Bopp at the time of this writing. We include (1) theoretical modeling of the gas/dust environment for Hale–Bopp, (2) a review of certain important relevant issues as posed from the results of comets observed before Hale–Bopp, and (3) a discussion of new Hale–Bopp observations which either shed new light or at least herald the possible shedding of new light in the not-too-distant future. Hale–Bopp is still being actively observed by the world's major observing programs. Despite the fact that we now only have an incomplete and preliminary picture of the observational evidence in this important area, there are already many interesting and important findings and questions.

The dust–gas environment for comet Hale–Bopp, especially when very active ($r \leq 1.5$ AU), is very different from the typical bright comets (e.g., P/Halley, and C/Hyakutake, 1996 B2). The large dust–gas production has a number of important consequences.

- The collisional fluid region is large.
- The resulting increased photochemical heating efficiency significantly increases gas outflow speeds and their variations with distance from the nucleus and with heliocentric distance.
- The large collision region will have an effect on the applicability of free-molecular-flow vectorial models which implicitly assume collisionless expansion.
- The UV opacity in the inner coma is not negligible, and could effect parent lifetimes and ion production especially for observations made with high spatial resolution.

– The high UV opacity will shield ionization within about 3000 km from the nucleus and within a tailward shadow (at r = 1 AU), and alter typical ion-neutral chemistry.
– The dust–gas interaction is strong and the region where it is important is large.
– This interaction yields fast micron-sized dust particles accelerated to nearly the gas speed. Even larger mm-size particles are accelerated to much larger velocities than the typical bright comet. Such effects will be important in understanding dust kinematics and in determining total dust-to-gas mass ratios from long wavelength IR and radio observations.

Preliminary observational results regarding dust–gas interrelations are also very interesting.

– The production of gas species and dust seems to be strongly influenced and sometimes dominated by localized active regions that rotate with the nucleus.
– The dust production from the active regions essentially turns-off on the night side.
– The gas production is reduced on the night side, but not completely inactive ($\sim$10% level in some species, but CO is uniformly active).
– There is evidence for extended sources not only for CO and H_2CO, as seen before, but also for CH_3OH, and HNC.
– At large distances ($r > 4$ AU) cometary CN seems to be mostly produced from HCN. At smaller distances ($r < 4$ AU) another source (or sources) appears to become active; suggestions for grains or other parent molecules (C_2N_2, CH_3CN) have been made.
– There is evidence for multiple sources for cometary C_2: photodissociation of C_2H_2 is an obvious candidate, and production of vibrationally excited C_2 from grains has been suggested.
– The new list of gas-jet species from visual-range CCD images of comet Hale–Bopp includes not only CN, C_2, and C_3 as in Halley, but also NH, and OH. Doppler-resolved radio observations indicate a similar behavior for CO, H_2CO, CH_3OH and H_2S. Similarities of behavior of HCN jets in Doppler-resolved radio observations and CN jets in CCD images, and the presence of gas jets in most commonly observed species, especially OH and NH, open to question the conclusion that previously observed CN jets necessarily implied production from an extended source of CHON grains. We examine here the pros and cons of three scenarios:

1. Gas-jet species are produced from CHON grains. Pros: Small organic grains (sub-μm) would be accelerated to nearly the gas speeds in both Halley and Hale–Bopp, accounting for the similar spatial geometry of dust and gas jets in Hale–Bopp but also their dissimilarity in Halley. Small organic grains (0.2 mm) should live long enough (1–2 $\times$ 10^5 seconds) for a comet at 1 AU (Lamy and Perrin, 1988) to provide a spatially extended source. Cons: The new evidence of gas jets in OH and NH in Hale–Bopp

indicates the gas-jet source may be rooted in the volatile fraction of the comet rather than in organic CHON grains. The similar visibility of OH jets and CN jets indicates that the relative source rates are similar in the jets source as in the comet in general. This similar relative abundance was also the case for the OH, CN and C_2 arc-structure seen in the tail of comet Hyakutake (C/1996 B2) which indicated production by typical fragments of the bulk nucleus rather than just CHON grains which are only one component of cometary material.

2. Gas-jet species are produced from volatile nucleus fragments (icy grains). Pros: This picture accounts for production of OH and NH which are considered to be produced from the volatile fraction of the cometary nucleus material, rather than from the organic CHON grains. A similar process has been invoked to explain the production of OH, in addition to CN and C_2 from a secondary source down in the tail of comet Hyakutake (C/1996 B2). Cons: In Hyakutake, both the lifetime of the particles (from the persistence of the source) and the motion of the source down the tail indicated that the parent fragment particles were large (mm-sized). In Hale–Bopp the gas-jet source particles are probably still closer to μm size rather than mm size based on the fast velocity and the fact that small icy grains do not survive more than about 10 000 km from the nucleus (Delsemme and Miller, 1971). Of course, the particles responsible for the jets in Hale–Bopp do not have to be the same as those responsible for the tail-side arc in Hyakutake.
3. Gas-jets are produced simply from localized concentrations of parent molecules. Pros: Because parent molecules are part of the general gas outflow, they, like the smallest grains, will move with the general gas outflow velocity. This would account for the velocity sorting for jets in Halley and for the lack of it in Hale–Bopp. The dusty-gas hydrodynamic models indicate that non-spherical asymmetries in the coma are frozen-in by a few nucleus-radii from the nucleus, therefore concentrations in angle of parent molecules could remain concentrated to large distances, thereby possibly maintaining a gas-jet identity. Cons: The gas concentrations which are similar to dust concentrations near the nucleus (10° half-cone-angle FWHM Gaussians) tend to broaden to ∼30° half-cone angle Gaussians by a few nucleus radii. Are these narrow enough to account for the well focused gas jets?

– A few more general and difficult questions regarding both gas and dust jets remain. It may be difficult to account for the constant projected radial propagation velocity of gas and dust jets (0.4 km s^{-1}) solely on geometrical projection effects (Larson, personal communication). This has larger consequences than the exact nature of the gas and dust jets. It is clear from the modeling presented here that the outflow velocities (0.7 to 2 km s^{-1}) predicted by dusty-gas dynamics models are consistent with those observed in Doppler

resolved measurements (Biver et al., 1997b; Colom et al., 1997). How can gas jets propagate at much smaller speeds than the actual gas outflow speed? Over the coming couple of years the wealth of important observational results for cornet Hale–Bopp will be filling the scientific literature. It is very likely that as a result of this singularly bright comet we will obtain definite answers to many of the above important questions about dust–gas interrelations. They have important consequences, not just those pertaining directly to our understanding of the behavior of processes occurring in the coma, but also, and more significantly, on our understanding of the detailed compositional and morphological make-up of comets, and how and where they were formed.

Acknowledgments

This research was supported by grants NAG 5-4714 and NAG 5-4381 from the NASA Planetary Atmospheres program. We thank and appreciate a several day email-conference among Steve Larson, Nalin Samarasinha, Dominique Bockelée-Morvan, and Dave Schleicher for helping to decide a compromise in setting (hopefully) useful 3D dusty-gas jet parameters with which to characterize the physics of the inner coma.

References

A'Hearn, M. F., Hoban, S., Birch, P. V., Bowers, C., Martin, R., and Kinglesmith, D. A.: 1956, *Nature* **324**, 649.

A'Hearn, M. F., Millis, R., Schleicher, D., Osip, D. D., and Birch, P.: 1995, *Icarus* **118**, 223.

Baum, W. A., Kreidl, T. J., and Schleicher, D. G.: 1992, *A. J.* **104**, 1216.

Biver, N., Bockelée-Morvan, D., Colom, P., Crovisier, J., Davies, J., Dent, W. R. F., Despois, D., Gèrard, E., Lellouch, E., Rauer, H., Moreno, R., and Paubert, G.: 1997a, *Science* **275**, 1915.

Biver, N., Bockelée-Morvan, D., Colom, P., Crovisier, J., Germain, E., Lellouch, E., Davies, J. K., Dent, W. R. F., Moreno, R., Paubert, G., Wink, J., Despois, D. C., Lis, D. C., Mehringer, D., Benford, D., Gardner, M., Phillips, T. G., Gunnarsson, M., Rickman, H., Winnberg, A., Bergman, P., Johansson, L. E. B., and Rauer, H.: 1997b, *Earth, Moon, and Planets* **78**, 5–11.

Bockelée-Morvan, D. and Crovisier, J.: 1985, *Astron. Astrophys.* **151**, 90.

Bockelée-Morvan, D. and Crovisier, J.: 1987, *Proc. Symp. on the Diversity and Similarity of Comets*, **ESA SP 277**, p. 235.

Bockelée-Morvan, D., Wink, J., Despois, D., Colom, P., Biver, N., Crovisier, J., Gautier, D., Gérard, E., Lellouch, E., Moreno, R., Paubert, G., Rauer, H., Davies, J. K., and Dent, W. R. F.: 1997, *Earth, Moon, and Planets* **78**, 67.

Boice, D. C., Benkhoff, J., and Laffont, C.: 1998, Paper presented at the *First International Conference on Hale–Bopp*, Tenerife, Canary Islands, 2–5 February 1998.

Budzien, S. A., Festou, M. C., and Feldman, P. D.: 1994, *Icarus* **107**, 164.

Cochran, A. L.: 1985, *Ap. J.* **289**, 388.

Cochran, A. L. and Schleicher, D. G.:1993, *Icarus* **105**, 235.

Cochran, A. L. and Trout, A. P.: 1994, *A. J.* **108**, 1471.

Colom, P., Gérard, E., Crovisier, J., Bockelée-Morvan, D., Biver, N., and Rauer, H.: 1997, *Earth, Moon, and Planets* **78**, 37–43.
Combi, M. R.: 1980., *Ap. J.* **241**, 830.
Combi, M. R.: 1987, *Icarus* **71**, 178.
Combi, M. R.: 1989, *Icarus* **81**, 41.
Combi, M. R.: 1994, *A. J.* **108**, 304.
Combi, M. R. and Cochran, A. L.: 1997, *Bull. A. A. S.* **29**, 1048.
Combi, M. R. and Delsemme, A. H.: 1980, *Ap. J.* **237**, 641.
Combi, M. R. and Delsemme, A. H.: 1986, *Ap. J.* **308**, 472.
Combi, M. R. and Feldman, P. D.: 1993, *Icarus* **105**, 557.
Combi, M. R. and Fink, U.: 1997, *Ap. J.* **484**, 879.
Combi, M. R. and Smyth, W. H.: 1988, *Ap. J.* **327**,1044.
Cosmovici, C. B., Schwarz, G., Ip, W.-H., and Mack, P.: 1988, *Nature* **332**, 705.
Crifo, J. F.: 1991, in R. L. Newburn et al. (eds.), *Comets in the Post-Halley Era*, Kluwer Academic Publishers, Dordrecht, p. 937.
Crifo, J. F., Itkin, A. L., and Rodionov, A. V.: 1995, *Icarus* **116**, 77.
Crifo, J. F., Itkin, A. L., and Rodionov, A. V.: 1997, *Icarus* **127**, 319.
Crifo, J. F., Itkin, A. L., and Rodionov, A. V.: 1998, submitted.
Delsemme, A. H.: 1982, in L. L. Wilkening (ed.), *Comets*, University of Arizona Press, Tucson, p. 85.
Delsemme, A. H. and Miller, D. C.: 1971, *Planet. Space Sci. D.C.* **19**, 1259.
DeZeeuw, D. L. and Powell, K. G.: 1992, *J. Comp. Phys.* **104**, 55.
DiSanti, M. A., Mumma, M.J., Dello Russo, N., Magee-Sauer, K., Rettig, T., and Novak, R.: 1998, Paper presented at the *First International Conference on Hale–Bopp*, Tenerife, Canary Islands, 2–5 February 1998.
Eberhardt, P. et al.: 1987, *Astron. Astrophys.* **187**, 481.
Festou, M. C.: 1981, *Astron. Astrophys.* **95**, 69.
Festou, M. C., Barele, O., Davidge, T., Stern, S. A., Tozzi, G. P., Womack, M., and Zucconi, J. M.: 1998, Paper presented at the *First International Conference on Hale–Bopp*, Tenerife, Canary Islands, 2–5 February 1998.
Fink, U., Combi, M. R., and DiSanti, M. A.: 1991, *Ap. J.* **383**, 371.
Finson, M. L. and Probstein, R. F.: 1968, *Ap. J.* **154**, 353.
Fitzsimmons, A. and Cartwright, I. M.: *MNRAS* **278**, 37.
Fulle, M., Bosio, S., Cremonese, G., Cristaldi, S., Liller, W., and Pansecchi, L.: 1993, *Astron. Astrophys.* **272**, 634.
Fulle, M., Mikuz, H., and Bosio, S.: 1997, *Astron. Astrophys.* **324**, 1197.
Gombosi, T. I.: 1986, *Exploration of Halle's Comet*, vol. 11, ESA SP-250, p. 167.
Gombosi, T. I., DeZeeuw, D. L., Häberli, R. M., and Powell, K. G.: 1996, *J. Geophys. Res.* **101**, 15333.
Gombosi, T. I., Hansen, K. C., DeZeeuw, D. L., Combi, M. R., and Powell, K. G.: 1997, *Earth, Moon, and Planets* **79**, 179–207.
Gombosi, T. I., Nagy, A. F., and Cravens, T. E.: 1986, *Rev. of Geophysics* **24**, 667.
Häberli, R. M., Combi, M. R., Gombosi, T. I., DeZeeuw, D. L., and Powell, K. G.: 1997, *Icarus* **130**, 373.
Häberli, R. M., Gombosi, T. I., DeZeeuw, D. L., Combi, M. R., and Powell, K. G.: 1997, *Science* **276**, 939.
Harris, W. M., Combi, M. R., Honeycutt, R. K., Mueller, B. E. A., and Scherb, F.: 1997, *Science* **277**, 676.
Hayward, T. L., and Hanner, M. S.: 1997, *Science* **275**, 1907.
Huebner, W. F. and Keady, J. J.: 1983, *International Conference on Cometary Exploration*, Hungarian Academy of Sciences, Budapest, p. 165.

Huebner, W. F., Snyder, L. E., and Buhl, D.: 1974, *Icarus* **23**, 580.
Huggins, W.: 1882, *Proc. Roy. Soc.* **33**, 1.
Ip, W.-H.: 1983, *Ap. J.* **264**, 726.
Ip, W.-H.: 1989, *Ap. J.* **346**, 475.
Jackson, W. M.: 1976, *The Study of Comets NASA SP-393*, NASA, Greenbelt, MD, p. 679.
Jackson, W. M.: 1991, in R. L. Newburn, Jr. et al. (eds.), *Comets in the Post-Halley Era*, Kluwer Academic Publishers, Dordrecht, p. 313.
Jewett, D. and Luu, J.: 1989, *A. J.* **97**, 1766.
Jewett, D. C. and Meech, K. J.: 1987, *Ap. J.* **317**, 992.
Jewett, D., Senay, M., and Matthews, H.: 1996, *Science* **271**, 1110.
Kabin, K., Gombosi, T. I., Combi, M. R., DeZeeuw, D. L., and Powell, K. G.: 1998, in preparation.
Keller, H. U. et al.: 1986, *Astron. Astrophys.* **187**, 807.
Keller, H. U., Marconi, M. L., and Thomas, N.: 1990, *Astron. Astrophys.* **227**, L1.
Khare, B. N., Sagan, C., Arakawa, E. T., Suits, F., Calcott, T A., and Williams, M. W.: 1984, *Icarus* **60**, 127.
Kidger, M. R., Serra-Ricart, M., Bellot-Rubio, L. R., and Casas, R.: 1996, *Ap. J.* **461**, L119.
Kitamura, Y.: 1986, *Icarus* **66**, 241.
Klavetter, J. J. and A'Hearn, M. F.: 1994, *Icarus* **107**, 322.
Konno, I., Huebner, W. F., and Boice, D. C.: 1993, *Icarus* **101**, 84.
Körösmezey, A. and Gombosi, T. I.: 1990, *Icarus* **84**, 118.
Korsun, P. P., Davis, S. P., Shavrina, A. V., Vasiljeva, I. E., Malanushenko, V. P., and Savanov, I. S.: 1997, *Earth, Moon, and Planets* **78**, 119–125.
Laffont, C., Rousselot, P., Clairemidi, J., and Moreels, G.: 1998, *Planet. and Sp. Sci.* (in press).
Laffont, C., Rousselot, P., Clairemidi, J., Moreels, G., and Boice, D. C.: 1997, *Earth, Moon, and Planets* **78**, 211-217.
Lamy, P. L. and Perrin, J.-M.: 1987, *Icarus* **76**, 100.
Lamy, P. and Perrin, J.-M.: 1988, *Icarus* **76**, 100.
Larson, S., and Hergenrother, C.: 1998, Paper presented at the *First International Conference on Hale–Bopp*, Tenerife, Canary Islands, 2–5 February 1998.
Lederer, S. M., Campins, H., Osip, D. J., and Schleicher, D. G.: 1997, *Earth, Moon, and Planets* **78**, 131–136.
Marconi, M. L. and Mendis, D. A.: 1984, *Ap. J.* **287**, 445.
Meier, R., Eberhardt, P., Krankowsky, D., and Hodges, R. R.: 1993, *Astron. Astrophys.* **277**, 677.
Millis, R. L. and Schleicher, D. G.: 1986, *Nature* **324**, 646.
O'Dell, C. R., Robinson, R. R., Krishna Swamy, S., McCarthy, P. J., and Spinrad, H.: 1988, *Ap. J.* **334**, 476.
Potter A. E. and DelDuca, B.: 1964, *Icarus* **3**, 103.
Probstein, R. F.: 1968, *Problems of Hydrodynamics and Continuum Mechanics*, Society for Industrial and Applied Mathematics, Philadelphia, p. 568.
Rauer, H., Arpigny, C., Boehnhardt, H., Colas, F., Crovisier, J., Jorda, L., Küppers, M., Manfroid, J., Rembor, K., and Thomas, N.: 1997, *Science* **275**, 1909.
Roussellot, P., Clairemidí, J., and Moreels, G.: 1994, *Astron. Astrophys.* **286**, 645–653.
Samarasinha, N. H. and Belton, M. J. S.: 1994, *Icarus* **108**, 103.
Samarasinha, N. H., Mueller, B. E. A., and Belton, M. J. S.: 1997–1999, *Earth, Moon, and Planets* **77**, 189–198.
Schleicher, D. G., Lederer, S. M, Millis, R. L., and Farnham, L.: 1997, *Science* **275**, 1913.
Schulz, R. and A'Hearn, M. F.: 1995, *Icarus* **115**, 191.
Schulz, R., A'Hearn, M. F., Birch, P. V., Bowers, C., Kempin, M., and Martin, R.: 1993a, *Icarus* **104**, 206.
Schulz, R., A'Hearn, M. F., and Samarasinha, N. H.: 1993b, *Icarus* **103**, 391.

Schulz, B., McFadden, L. A., Chamberlin, A. B., A'Hearn, M. F., and Schleicher, D. G.: 1994, *Icarus* **109**, 145.
Sekiguchi, T., Watanabe, J., Fukushima, H., Yamamoto, T., and Yamamoto, N.: 1997, *Earth, Moon, and Planets* **78**, 143–148.
Senay, M. C., Rownd, B., Dickens, J. E., DeVries, C. H., Schloerb, F. P., Mayhew, L., Yuen, L., and Mauskopf, P.: 1998, Paper presented at the *First International Conference on Hale–Bopp*, Tenerife, Canary Islands, 2–5 February 1998.
Smyth, W. H., Combi, M. R., Roesler, F. L., and Scherb, F.: 1995, *Ap. J.* **440**, 349.
Thomas, N. and Keller, H. U.: 1990, *Astron. Astrophys.* **249**, 258.
Wagner, R. M. and Schleicher, D. G.: 1997, *Science* **275**, 1918.
Wallace, L. V. and Miller, F. D.: 1958, *A. J.* **63**, 213.
Weaver, H. A., Feldman, P. D., A'Hearn, M. F., Arpigny, C., Brandt, J. C., Festou, M. C., Haken, M., McPhate, J. B., Stern, S. A., and Tozzi, G. P.: 1997, *Science* **275**, 1900.
Whipple, F. L. and Huebner, W. F.: 1976, *Ann. Rev. Astron. Astrophys.* **14**, 143.
Wink, J., Bockelée-Morvan, D., Despois, D., Colom, P., Biver, N., Crovisier, J., Gérard, E., Lellouch, E., Davies, J. K., Dent, W. R. F., and Jorda, L.: 1997, *Earth, Moon, and Planets* **78**, 63.
Womack, M., Festou, M. C., and Stern, S. A.: 1997, *A. J.* **114**, 2789.
Wyckoff, S., Tegler, S., Wehinger, P. A., Spinrad, H., and Belton, M. J. S.: 1988, *Ap. J.* **325**, 927.
Yamamoto, T.: 1981, *Moon and Planets* **24**, 453.